Tuning the Photocatalytic Activity of Layered Perovskite Niobates by Controlled Ion Exchange and Hydration

*Calin Ladasiu, Natalia Kulischow, Roland Marschall[#,]**

Abstract. Dion-Jacobson type layered perovskite niobium oxides $KCa_2Nb_3O_{10}$ and $KSr_2Nb_3O_{10}$ were prepared *via* molten salt method, and the potassium cations were exchanged by protons using nitric acid. Different degrees of proton exchange were adjusted, and the dependence of photocatalytic activity for hydrogen evolution on proton exchange was investigated. Moreover, proton exchange leads to different amounts of water incorporated into the interlayer spaces, also influencing photocatalytic performance significantly. Decoupling water intercalation and proton exchange, the photocatalytic activity of proton exchanged $KCa_2Nb_3O_{10}$ and $KSr_2Nb_3O_{10}$ can be revealed and tailored for maximum activity.

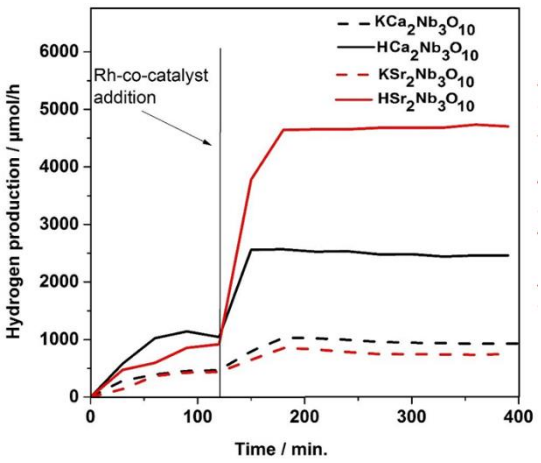

Keywords: layered perovskites, proton exchange, photocatalysis, hydrogen evolution,

Dr. C. Ladasiu, N. Kulischow, Prof. R. Marschall
Institute of Physical Chemistry,
Justus-Liebig-University Giessen,
D-35392 Giessen, Germany
#present address: Department of Chemistry,
University of Bayreuth, 95447 Bayreuth, Germany
* Email: Roland.marschall@uni-bayreuth.de , ORCID: 0000-0002-1057-0459

1. Introduction

Layered Dion-Jacobson perovskites represent an attractive class of materials for photocatalytic water splitting due to their particular structure and properties compared with other photocatalysts.[1–9] Originally synthesized by Dion,[1] the general formula of these compounds can be expressed as A'[$A_{n-1}B_nO_{3n+1}$], where A' is an alkali metal, A is an alkaline earth or rare earth metal, and B is a pentavalent metal, mainly niobium or tantalum.[5] The structure of these compounds consists of stacked, negatively charged perovskite sheets, interleaved with A' cations.[3,4] These materials exhibit a series of interesting properties such as superconductivity, dielectric behavior, photoluminescence, good electron conductivity, ion exchange, and intercalation depending on composition.[9–13] Furthermore, they are also known to have a higher photocatalytic activity under UV light compared to bulk-type photocatalysts such as TiO_2,[2,4] although exhibiting often a larger band gap.

This higher photocatalytic activity is ascribed to their layered structure that gives the ability to intercalate molecules in the interlayer space,[4] and to the fact that the interlayer space is a potential reaction site for water splitting.[10] This fact is also valid for other layered oxide photocatalysts, we recently showed that ion exchange and doping into layered titanates can alter their absorption and photocatalytic activity.[14] Furthermore, the layered structure of Dion-Jacobson perovskites can also promote the separation of photo-generated charges resulting in improved activity for hydrogen generation.[13]

Due to their layered structure and relative large interlayer space, these materials can be easily modified by exchanging the A' cation with other alkali metals or protons.[5] In particular, proton exchanged layered perovskites were shown to exhibit significant increase in photocatalytic activity compared to the parent compound.[2,4] Such increase is attributed to the hydration of the interlayer that leads to an increase of the interlayer space, resulting in the ability to further intercalate molecules such as alcohols used as sacrificial agents.[2,3]

In this work, a series of layered Dion-Jacobson oxide perovskites (A'[$A_2Nb_3O_{10}$] where A' = K and A = Ca, Sr) was prepared using a molten salt synthesis method.[6] The compounds were then proton-exchanged, and their photocatalytic activity for hydrogen production was investigated. Although the photocatalytic activity for hydrogen production of $KCa_2Nb_3O_{10}$ (with different degrees of H^+ exchange) has been previously reported by Domen *et al.*,[2] to the best of our knowledge, the influence of the degree of proton exchange and subsequent hydration on the photocatalytic activity of $KSr_2Nb_3O_{10}$ for hydrogen evolution and a comparison to $KCa_2Nb_3O_{10}$ has not been yet investigated. We reveal that the photocatalytic activity of proton-exchanged $KSr_2Nb_3O_{10}$ is significantly improved compared to the parent material, and is directly dependent on the degree of proton exchange and subsequent hydration.

2. Experimental Section

2.1 Reagents and Materials

All chemicals used were of analytical grade and used as received. $CaCO_3$ (Grüssing, 99.0 %), HNO_3 (Sigma-Aldrich, 65 %), KCl (Grüssing, 99.0 %), K_2CO_3 (Grüssing, 99.0 %), methanol (J. T. Baker, a. g.), Na_3RhCl_6 (Sigma-Aldrich, 99.9 %), Nb_2O_5 (Fluka, 99.9 %), perchloric acid (Sigma-Aldrich, 70 %), $SrCO_3$ (Grüssing, 99.0 %), $Sr(NO_3)_2$ (Acros Organics, 99.9 %).

2.2 Photocatalyst Preparation

The layered niobium oxides $KCa_2Nb_3O_{10}$ and $KSr_2Nb_3O_{10}$ were synthesized from carbonate or nitrate precursors and niobium pentoxide using a molten salt method described elsewhere.[6]

The proton exchange was carried out by stirring the compounds in 1M HNO_3 solution at 60 ºC for up to 18 hours with intermediate solution exchange: Stirring of the compounds in 1M HNO_3 at room temperature for 30 min causes a proton exchange of 60 %. Heating the mixture up to 60 °C and stirring for 1 h results in 80 % exchange. Higher degrees and the completion of exchange is achieved by stirring the mixture up to 18 h with intermediate solution exchange after every 3h.

For the photocatalytic activity study with different degrees of proton exchange, 500 mg of

$KCa_2Nb_3O_{10}$ or $KSr_2Nb_3O_{10}$ was stirred at room temperature and at 60 °C with 40 mL 1M HNO_3 for different time intervals. The completion and the degree of proton exchange was monitored by energy-dispersive X-ray analysis (EDX).

2.3 Characterization

X-ray diffraction patterns were acquired on a PANalytical MPD diffractometer using Cu-K_α radiation (λ = 0.1541 nm) in the 2θ range from 5° to 30°. Interlayer spaces were calculated from XRD measurements using the 00l reflections. The EDX elemental analysis was conducted on a Philips LEO Gemini 982 field emission SEM at 20 kV accelerating voltage. UV-VIS diffuse reflectance measurements were done on a Perkin Elmer Lambda 750 spectrometer equipped with a Praying-Mantis accessory. The reflectance spectra were recorded between 200 and 500 nm using $BaSO_4$ as reference. Raman spectra were acquired on a SENTERRA dispersive Raman microscope from Bruker Optics equipped with an Olympus (MPlan N 50x) objective and an Nd:YAG laser (λ = 532 nm, P = 2.0 mW). Thermogravimetric analysis (TGA-DTA) was performed on a NETZSCH STA 409 PC/PG instrument using an Al_2O_3 crucible under the following conditions: 30 mL/min. Ar gas flow, temperature range between 25 °C and 1000 °C, heating rate 5 °K/min. Water physisorption was measured at 20 °C in a water bath using an Autosorb iQ2 from Quantachrome Instruments. All samples were degassed at 120 °C in vacuum beforehand.

2.4 Hydrogen production - Experimental Setup and Procedure

The photocatalytic hydrogen production using the proton-exchanged materials was carried out in a double-walled inner irradiation-type quartz reactor connected to a homemade closed gas evolution system.[6]

To prevent any thermal catalytic effect, the reactor was cooled down to 10 °C by circulating water from a thermostat (Lauda) using a double walled quartz jacket. A 350 W Hg immersion lamp (UV-Consulting, Peschl) was used as light source. As carrier gas for the reaction products high purity argon was used with a flow rate set at 25 mL/min controlled by a Bronkhorst mass flow controller. For the detection of the evolved hydrogen, a Shimadzu GC-2014 gas chromatograph was used equipped with a thermal conductivity (TCD) detector and RESTEK ShinCarbon ST 100/120 column. The column was kept at 35 °C throughout the measurement. The elution time for H_2 was 1 minute.

In a typical experiment 0.3 g photocatalyst was suspended (under sonication) in 600 mL aqueous methanol (10 % v/v) solution. The solution initial pH was adjusted to 3 with perchloric acid. Prior to irradiation, the system was purged with argon at 100 mL/min to ensure complete air removal. The reaction was allowed to proceed for two hours. Afterwards, Rh was *in-situ* photo-deposited (0.05 wt.-% Rh loading) on the catalyst from Na_3RhCl_6 (1.7 mL) introduced in the reactor with a syringe through a reactor inlet and rubber sealing. After 30 min purging, the irradiation continued for another five hours.

3. Results and discussion

The degree of proton exchange and the completion of exchange was monitored by EDX and is summarized in Table S1 of the supplementary information. In the beginning, the proton exchange takes place exceedingly fast. Stirring of the compounds in 1M HNO_3 at room temperature for 30 min causes a proton exchange of 60 %. Heating the mixture up to 60 °C and stirring for 1 h results in 80 % exchange. From this point on the exchange of K^+ with H^+ slows down. Higher degree and the completion of exchange is achieved by stirring the mixture up to 18 h with intermediate solution exchange after every 3 h.

Figure 1 shows the powder XRD patterns of the 100 % proton exchanged compounds – denoted $HSr_2Nb_3O_{10}$ and $HCa_2Nb_3O_{10}$ – along with the XRD patterns of the starting materials. In both cases, two small reflections (002), (004) for $HSr_2Nb_3O_{10}$ and (001), (002) for $HCa_2Nb_3O_{10}$ due to the layered structure can be seen between 5 and 15° 2θ in the diffractograms of the parent compounds.

Further analysis of the diffraction pattern of $HSr_2Nb_3O_{10}$ reveals a shift to lower 2θ angles of the (002) and (004) reflections (Fig. 1a) that are indicative of an increase of the interlayer space.

However, in the diffraction pattern of $HCa_2Nb_3O_{10}$ (Fig. 1b), a shift to higher 2θ angles of the (001) and (002) reflections can be seen suggesting a contraction of the interlayer spacing.

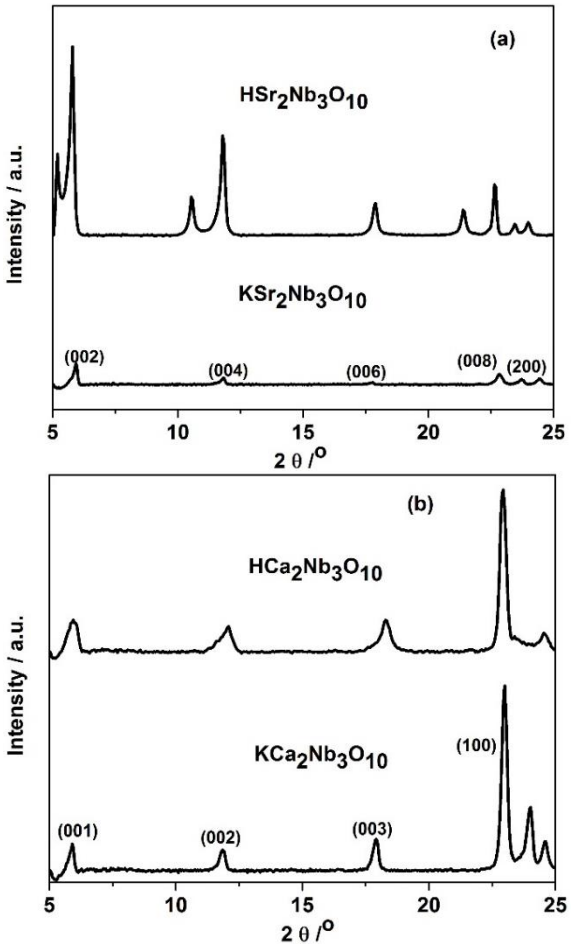

Figure 1. *XRD patterns of the proton exchanged compounds compared with the original material for a) $KSr_2Nb_3O_{10}$, and b) $KCa_2Nb_3O_{10}$.*

The increase of the interlayer spacing observed for $HSr_2Nb_3O_{10}$ can be attributed to the hydration[3,8] of the structure that leads to water intercalation following complete proton exchange. The change in the interlayer spacing is dependent on the degree of proton exchange as shown below.

Figure 2a shows the change in the interlayer length along the c-axis of $KSr_2Nb_3O_{10}$ with different percentages of proton exchange. It can be observed that the interlayer space increases with increasing percent of proton exchange and such increase is attributed to water intercalation following hydration. However, this increase is not continuous. This could be due, as Domen *et al.* suggested, to the hydration occurring in two steps.[2] First step represents a continuous hydration up to 60 % proton exchange (Fig. 2a) when the change in the interlayer spacing is most prominent. Further proton exchange results in a slight contraction of the interlayer space when reaches 80 % protonation (possibly due to the more advanced replacement of the potassium cations with the smaller protons). After that, a second step of hydration occurs leading to further increase of the interlayer space (Fig. 2a).

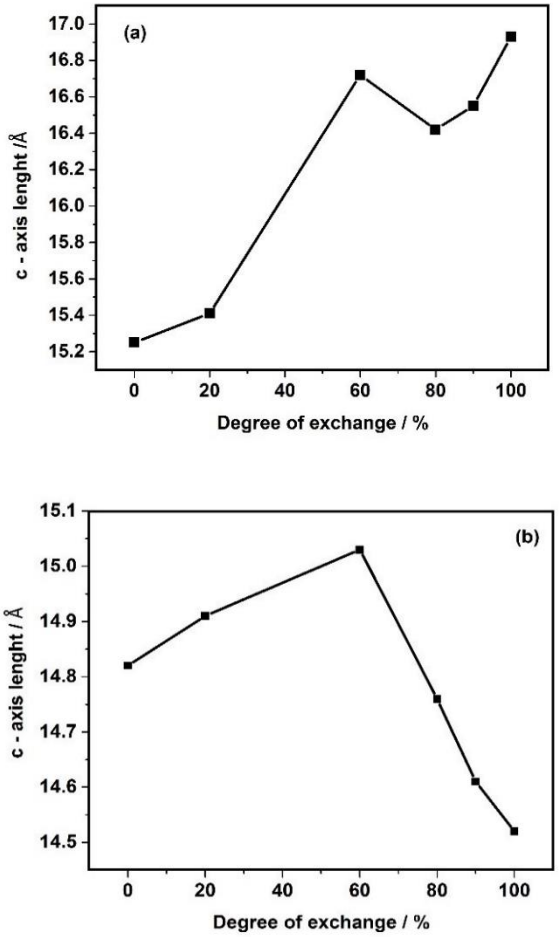

Figure 2. *C-axis length change following proton exchange: a) $KSr_2Nb_3O_{10}$, b) $KCa_2Nb_3O_{10}$.*

Such hydration behavior implies the existence of two types of water in the structure. This is confirmed by the two water loss steps at 289 °C (0.014 mmoles H_2O) and 450 °C (0.075 mmoles H_2O) observed in the TGA-DTA curves of $HSr_2Nb_3O_{10}$ (Figure 3).

By comparison, only one water loss step at 289 °C (0.101 mmoles H_2O) can be seen in the TGA-DTA curves of $HCa_2Nb_3O_{10}$.

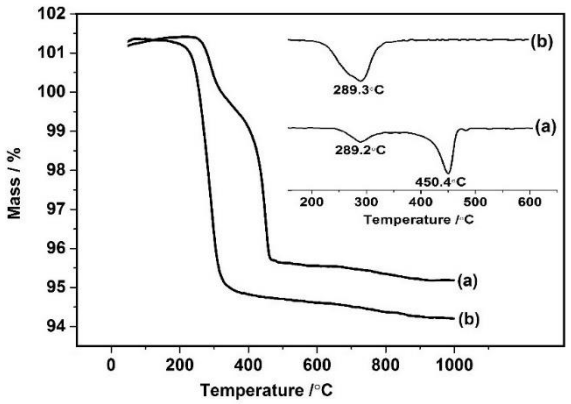

Figure 3. *TGA and DTA (inset) curves of (a) $HSr_2Nb_3O_{10}$ and (b) $HCa_2Nb_3O_{10}$.*

TGA and XRD have also been performed on the $KSr_2Nb_3O_{10}$ and $KCa_2Nb_3O_{10}$ having different degrees of proton exchange (Figure S1 supplementary data) and the observations are summarized below. For $KSr_2Nb_3O_{10}$, at 0 and 20 % H^+ exchange, no weight loss was observed in the TGA thermograms. The XRD patterns show the presence of layer peaks. At 60 and 80 % H^+ exchange, two weight loss steps can be observed (around 150 ºC and 300 ºC) in the TGA thermograms and the XRD patterns show low intensity layer peaks. Both TGA and XRD suggest intercalation and structure decomposition water loss.

As the degree of protonation increases to 90 and 100 %, only one weight loss step is observed around 300 ºC in the TGA thermograms, and the layer peaks can no longer be observed in the XRD diffractograms. The loss of intercalated water leads to the collapse of the interlayer space and the water loss suggests structural changes due to decomposition,[15] as it can be observed in the XRD diffractograms of the 60 and 100 % H-exchanged compounds (after TGA) where the layered peaks can no longer be observed. This trend could also be confirmed by water physisorption measurements (Table S2), where the amounts of adsorbed water drops significantly after 60 % proton exchange, indicating structure collapse.

For $KCa_2Nb_3O_{10}$, up to and including 60 % H^+ exchange, no weight loss is observed in the TGA thermograms; layer peaks are present in the XRD diffractograms. At 80, 90 and 100 % proton exchange, one weight loss step was observed at a lower temperature compared to the weight loss steps observed in the TGA thermograms of $KSr_2Nb_3O_{10}$ with 90 and 100 % H exchange. The absence of the layer peaks in the XRD diffractograms of the compounds at and above 80 % H^+ exchange also suggest the collapse of the interlayer space.

For $HCa_2Nb_3O_{10}$, in contrast to the observations made by Domen *et al.*,[2] after an initial increase in the interlayer spacing (at 20 % and 60 % proton exchange) a decrease was observed above 60 % proton exchange (Fig. 2b). Based on these observations, it can be concluded that some water intercalation may occur in this compound up to 60 % proton exchange. After that, as the degree of proton exchange increases, no hydration/water intercalation is observed. Therefore, as reported by Chen *et al.*[7] the more advanced replacement of the bigger alkali metal cation with protons can lead to a contraction of the interlayer space. This has a negative effect on the intercalation of water in the interlayer galleries. The contraction of the interlayer space is suggested by the shift of the diffraction peaks to higher 2θ angles (Fig. 1b) above 60 % proton exchange. However, some water intercalation does occur during the course of the photocatalysis experiment (shift to lower *2θ* angles of the (001) and (002) peaks – Figure S3 supplementary data) and can account for the better activity of the 100 % proton exchanged compound when compared with the parent compound (Figure 7).

Figure 4 shows the XRD patterns of $KSr_2Nb_3O_{10}$ with different percentages of proton exchange. It can be seen that at 80 % H^+ exchange, the (002) and (004) reflections start to split in two, the separation being complete after 90-100 % exchange. This points to the existence of two phases – hydrated and dehydrated $HSr_2Nb_3O_{10}$ – marked with asterisks in Figure 4. To the best of our knowledge, this is the first time such hydration behavior and the coexistence of two (hydrated and dehydrated) phases, was observed in $HSr_2Nb_3O_{10}$. Reference samples (fully dried in a vacuum furnace or fully hydrated) have been prepared and their patterns are shown to indicate the respective reflections.

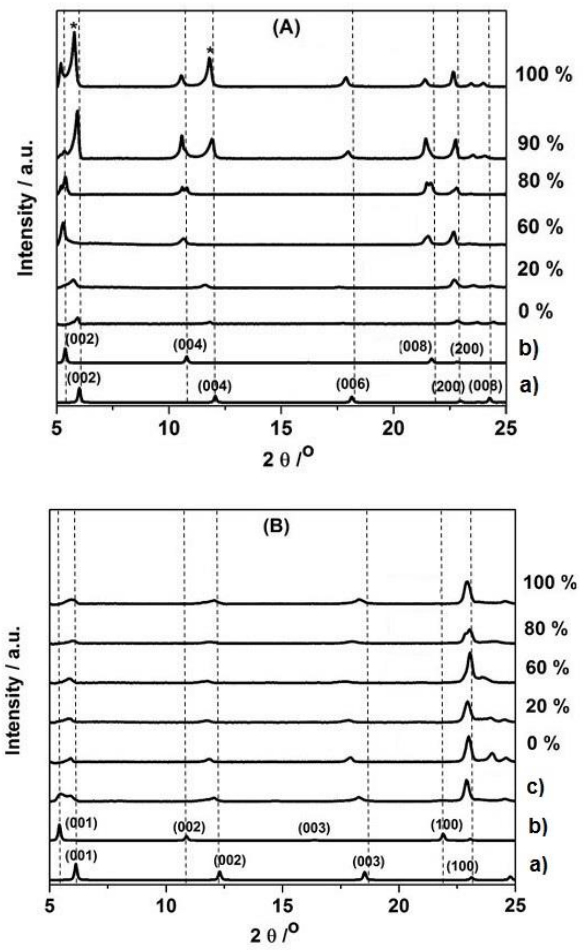

Figure 4. *XRD patterns of (A) $KSr_2Nb_3O_{10}$ and (B) $KCa_2Nb_3O_{10}$ with different percentages of proton exchange and: (a) reference pattern dry proton exchanged compound, (b) reference pattern fully hydrated proton exchanged compound, (c) $HCa_2Nb_3O_{10}$ after hydration.*

Furthermore, the intensity of the (002) and (004) reflections increases with the degree of exchange and could be related to the change in the interlayer spacing. The (006) reflection (present in the dehydrated form) disappears when the exchange reaches 60 %. As the exchange continues and the second (dry phase) starts to form (Figure 4), the (006) peak can again be clearly seen.

As it was shown above, the proton-exchanged Ca^{2+} and Sr^{2+} niobates exhibit different hydration/water intercalation behavior. Norby *et al.*[16] showed that there is a correlation between the hydration enthalpy of the perovskites and the differences in electronegativity between the A and B cations (in our case A = Sr, Ca and B = Nb) which can be represented by the formula:

$$\Delta H \text{ (kJ mol}^{-1}) = 400\Delta X_{\mathbf{B-A}} - 180 \qquad (1)$$

where: ΔH = hydration enthalpy (kJ mol^{-1}), $\Delta X_{\mathbf{B-A}}$ = the difference in the Allred–Rochow electronegativity between the B and A cations. The above formula was used to calculate the hydration enthalpy of Sr^{2+} and Ca^{2+} containing niobium oxides. The results show that the calcium niobate has more negative hydration enthalpy (- 104 kJ mol^{-1}) than the strontium niobate (- 84 kJ mol^{-1}), thus the hydration enthalpy is thermodynamically more favourable. This can explain why the calcium containing niobates (both bulk and proton exchanged) incorporate more water than the strontium containing ones (bulk and proton exchanged), as seen in water adsorption studies done on the materials and summarized in Table S2 supplementary information. However, based on TGA and XRD observations, even if the proton-exchanged calcium niobates take up more water, in the proton-exchanged strontium compounds the water intercalates between the layers, whereas in the calcium niobates remains mainly as hydration water or some may intercalate depending on the degree of proton exchange.

A possible explanation of this water intercalation behavior of the proton-exchanged compounds can be derived from the structural changes that occur after acid treatment. ^{93}Nb NMR studies have shown that upon proton exchange, the local environments of the niobium sites at the interface of the layers change when compared with the parent compounds, according to Wang *et al.*.[17,18] The proton exchange leads to a change in the Nb-O bonds length and also bond angles. Based on our observations, such changes could affect the water intercalation in between the perovskite layers of the proton-exchanged compounds.

Figure 5 shows the Raman spectra of $KCa_2Nb_3O_{10}$ and $KSr_2Nb_3O_{10}$ with bands characteristic for a perovskite structure. The bands at 930-940 cm^{-1} represent the Nb=O terminal stretching mode, the bands at 680-770 cm^{-1} and 530-570 cm^{-1} represent the edge-shared octahedral NbO_6 symmetric stretching modes.[19] The bands at 430-500 cm^{-1} are assigned to the edge-shared octahedral NbO_6 antisymmetric stretching modes.[19] A small band at ~ 840 cm^{-1} can also be seen in the spectrum of $KCa_2Nb_3O_{10}$ assigned to the number of perovskite layers.[19]

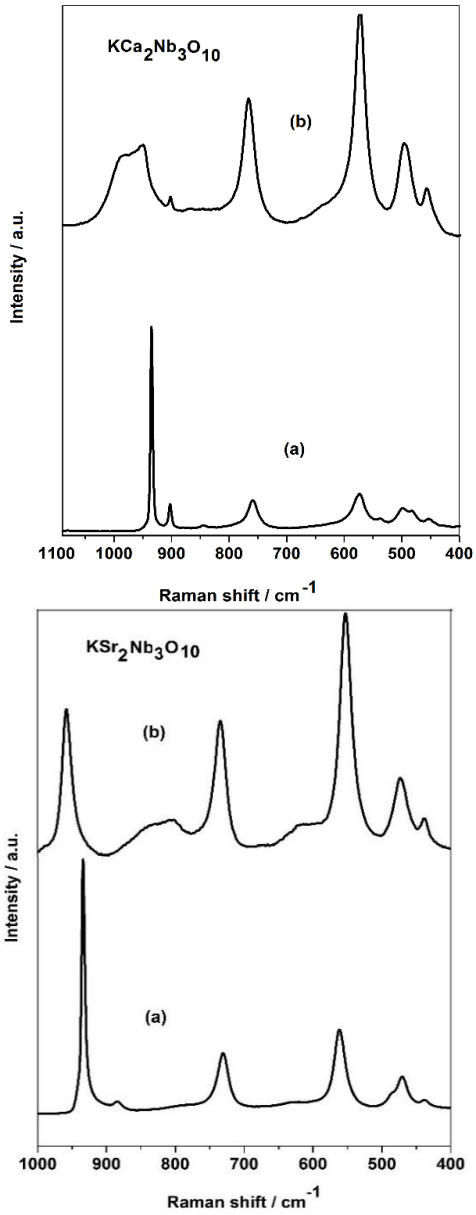

Figure 5. *Raman spectra of $KCa_2Nb_3O_{10}$ and $KSr_2Nb_3O_{10}$ (a) before and (b) after 100% proton exchange.*

The Raman spectra of both $KCa_2Nb_3O_{10}$ and $KSr_2Nb_3O_{10}$ show an extra Nb=O terminal stretching mode represented by the bands at 890-910 cm^{-1} that arise due to unequal Nb=O bond lengths.

Figure 5 also shows the Raman spectra of the compounds after proton exchange. It can be observed that in the case of $HCa_2Nb_3O_{10}$ the sharp peak at ~ 940 cm^{-1} is shifted and splits in two bands at ~ 960 cm^{-1} and at ~ 980 cm^{-1} and the peak at ~ 840 cm^{-1} disappears. According to Jehng *et al*. [16], this happens during dehydration of the proton-exchanged compound. Therefore, it seems that the material is not hydrated when 100 % proton exchanged, or it could be due to the contraction of the interlayer spacing as shown in Figure 2b. In addition, the disappearance of the peak at ~ 840 cm^{-1} might suggest a change in the number of perovskite layers.

The Raman spectrum of $HSr_2Nb_3O_{10}$ shows a broad peak at ~ 800 cm^{-1} that can be assigned to the hydrated form by analogy with the Raman spectrum of hydrated $HCa_2Nb_3O_{10}$ [16], due to an anti-symmetric stretching mode of Nb-O bond.[4]

In both cases, in the Raman spectra of the protonated compounds, the peak positions are maintained except for the peak at ~ 940 cm^{-1} for $HCa_2Nb_3O_{10}$ and the new peak at ~ 800 cm^{-1} for $HSr_2Nb_3O_{10}$ suggesting that the local structure for both compounds remains largely unchanged after proton exchange.

Figure 6 shows the Tauc plots of the proton-exchanged niobates. Table 1 summarises the bang gap energies, the conduction band potentials and steady state H_2 evolution of parent and proton exchanged $KCa_2Nb_3O_{10}$ and $KSr_2Nb_3O_{10}$. It can be observed that when compared with the parent compounds, the band gap of $HSr_2Nb_3O_{10}$ is increased by 0.1 eV whereas the band gap of $HCa_2Nb_3O_{10}$ decreases by the same value. According to Matsumoto *et al.*,[20] there is an empirical relationship between the conduction band potential (E_{CB}) and the band gaps (E_g) of metal oxide semiconductors having d^0 and d^{10} orbitals, described by the formula below:

$$E_{CB} = 1.23 - E_g/2 \qquad (2)$$

Using this formula it is possible to estimate the conduction band potential of the materials before and after proton exchange. The potential of the conduction band edge of $HSr_2Nb_3O_{10}$ becomes slightly more negative and the conduction band edge of $HCa_2Nb_3O_{10}$ becomes slightly more positive after proton exchange (Table 1). However, the band gap energies for the $HSr_2Nb_3O_{10}$ are still lower than for $HCa_2Nb_3O_{10}$, the conduction band edge potential being more negative than for $HSr_2Nb_3O_{10}$.

Nevertheless, as shown in Table 1, $HSr_2Nb_3O_{10}$ has the highest photocatalytic activity. This could be due, among other factors, to the fact

that the smaller band gap of $HSr_2Nb_3O_{10}$ makes up for the somewhat more positive conduction band egde potential in determining the hydrogen production efficiency as suggested by Maeda *et al*.[4] and also by shifting the potential to more negative values the driving force for hydrogen production is increased. The trend in hydrogen evolution is in agreement also with earlier reports by Domen et al..[2]

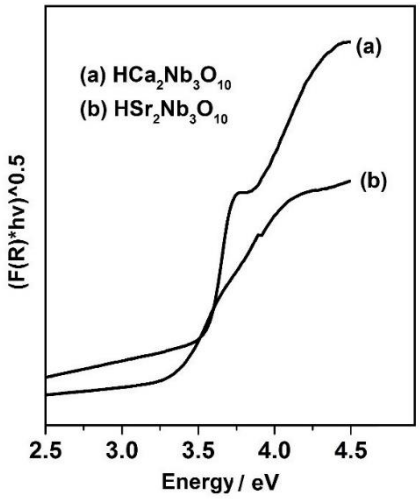

Figure 6. *Tauc plots of the 100% proton exchanged layered niobates.*

Figure 7 shows the photocatalytic hydrogen evolution with the 100 % proton-exchanged layered niobates from water/methanol solution compared with the parent compounds. All samples show photocatalytic activity without the addition of a co-catalyst. The photocatalytic activity of the proton-exchanged compounds, after co-catalyst addition, is significantly improved, $HSr_2Nb_3O_{10}$ having the highest activity and an almost eightfold increase compared to the starting compound.

As it was mentioned before, the observed higher photocatalytic activity of $HSr_2Nb_3O_{10}$ could be due to the expansion of the interlayer space along the c-axis[20,21] with the percentage of protonation and subsequent hydration. Figure 8a shows the dependence of the H_2 evolution rate (steady-state rates) on the degree of proton exchange of $KSr_2Nb_3O_{10}$. It can be observed that the H_2 evolution rate increases significantly after 80 % proton exchange that also corresponds to the onset of the second step of hydration. This increase can be ascribed to the further expansion of the interlayer space as shown in Figure 2a due to the start of the second hydration step. Therefore, as the degree of exchange increases, with the second step of hydration, more water molecules are intercalated.

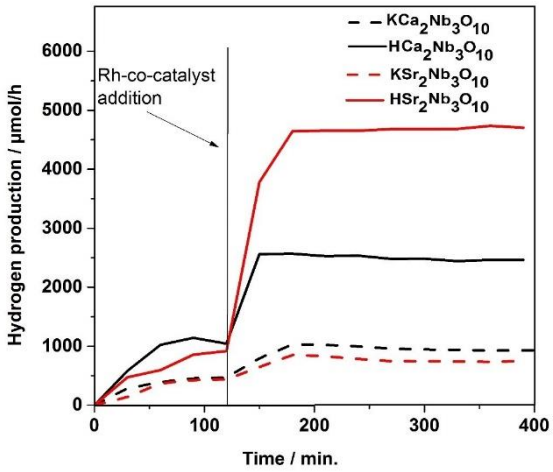

Figure 7. *Hydrogen evolution rates of the 100 % proton exchanged materials compared with the parent compounds (0.3 g catalyst, 10% MeOH).*

Table 1. Band gap energies, conduction band potentials and steady state H_2 evolution of 100 % proton exchanged $KCa_2Nb_3O_{10}$ and $KSr_2Nb_3O_{10}$.

Material	Band-gap energy / eV	Band-gap energy parent material / eV	Conduction band potential / V (*vs.* NHE at pH 0)	Conduction band potential parent material / V (*vs.* NHE at pH 0)	Steady rate of H_2 evolution / µmol/h (100 % proton exchanged, 0.3g)
$HCa_2Nb_3O_{10}$	3.5	3.6	- 0.52	- 0.57	2500
$HSr_2Nb_3O_{10}$	3.3	3.2	- 0.42	- 0.37	4700

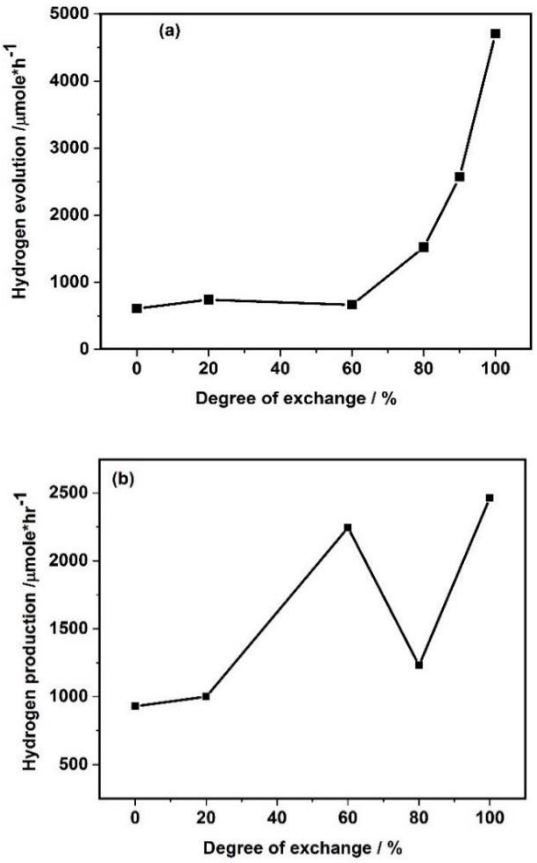

Figure 8. *Dependence of the steady-state rate of H_2 evolution on the degree of H^+ exchange for $KSr_2Nb_3O_{10}$ (a) and $KCa_2Nb_3O_{10}$ (b).*

As Domen *et al*. suggested,[2] during the expansion of the interlayer space, methanol molecules also start to intercalate and the increase in hydrogen production is attributed to the oxidation of methanol at the interlayer space. Figure 8b shows the dependence of the H_2 evolution rate (steady-state rates) on the degree of proton exchange of $KCa_2Nb_3O_{10}$. After an initial increase, the hydrogen production starts to decrease with the increase of the degree of proton exchange (80 %) and it can be correlated with the decrease in the interlayer spacing following protonation (Figure 2b). At 100 % proton exchange, the hydrogen production increase to the level reached by the 60 % exchanged sample.

Thus, compared with $HCa_2Nb_3O_{10}$, the fact that $HSr_2Nb_3O_{10}$ has higher activity than the former can be attributed mainly to the increase of interlayer space following proton exchange. This allows according to Domen *et al.* for more water and methanol to be intercalated and more efficient utilisation of the interlayer space for photocatalytic reactions.[2]

Another factor that can influence the photocatalytic activity of these compounds can be the distortion of the NbO_6 octahedra in the perovskite layers. ^{93}Nb NMR studies on the bulk and proton exchanged materials have shown that the distortion of the NbO_6 octahedra in $KCa_2Nb_3O_{10}$ is relaxed when the potassium ions are exchanged with protons due to the change in the local environments of the niobium sites at the interface of the layers.[17] In case of Sr containing compounds, the NbO_6 octahedra is distorted following proton exchange.[18] The distortion of the octahedra can generate internal electric fields due to dipole moments and such electric fields can mitigate the effect of the recombination of charge carriers thus improving the photocatalytic activity.[18,22]

Post-catalytic XRD analysis reveals a single hydrated $HSr_2Nb_3O_{10}$ phase (Figure S3 supplementary information). This suggest that the hydration continues during photocatalysis until only the hydrated phase remains, and this has a positive effect on the photocatalytic activity, which also accounts for better activity compared with the parent material.

Based on the above it can be concluded that in the case of $HSr_2Nb_3O_{10}$ the internal electric fields, the shift to more negative values of the conduction band edge together with the larger interlayer space (meaning more water and water/methanol accesible in the interlayer space) seem to have a positive effect on the photocatalytic hydrogen generation.

4. Conclusions

In this work layered Dion-Jacobson oxide perovskites $KCa_2Nb_3O_{10}$ and $KSr_2Nb_3O_{10}$ were prepared using a molten salt synthesis method followed by the exchange of the potassium ions by protons using nitric acid. The proton-exchanged compounds were analyzed using X-ray diffraction,, Raman and UV/VIS spectroscopy, thermogravimetric analysis and water vapor physisoprtion. The XRD analysis after proton exchange showed an increase in the interlayer spacing for $HSr_2Nb_3O_{10}$. For $HCa_2Nb_3O_{10}$ however, and after an initial

increase, a decrease in the interlayer spacing was observed. Such change was found to be dependent on the degree of proton exchange. The increase in the interlayer spacing of $HSr_2Nb_3O_{10}$ is due to the hydration that occurs in two steps suggesting the presence of two types of hydration water in the $HSr_2Nb_3O_{10}$. Hydrogen production experiments with the proton exchanged materials showed an increase in the photocatalytic activity after proton exchange, with the $HSr_2Nb_3O_{10}$ having the highest hydrogen production rate. This is ascribed to combined effects between the increased interlayer space, distortion of the octahedra generating internal electric fields and reducing the recombination of charge carriers.

Author Contributions. The manuscript was written through contributions of all authors. All authors have given approval to the final version of the manuscript.

Acknowledgement. We acknowledge financial support by the BMBF (Bundesministerium für Bildung und Forschung), research project DuaSol (03SF0482D). We thank Dr. Jana Timm for water adsorption and Hubert Woerner, Felix Badaczewski and Kevin Turke for thermogravimetric analysis (all Justus-Liebig-University Giessen). R.M. gratefully acknowledges funding in the Emmy-Noether program (MA 5392/3-1) of the German Research Foundation DFG.

References

[1] M. Dion, M. Ganne, M. Tournoux, *Mater. Res. Bull.* **1981**, *16*, 1429–1435.
[2] K. Domen, E. Yasuo, K. Junko, *Res. Chem. Intermed.* **1994**, *20*, 895–908.
[3] M. Sato, J. Watanabe, K. Uematsu, *J. Solid State Chem.* **1993**, *107*, 460–470.
[4] K. Maeda, T. E. Mallouk, *J. Mater. Chem.* **2009**, *19*, 4813.
[5] I. A. Rodionov, I. A. Zvereva, *Russ. Chem. Rev.* **2016**, *85*, 248–279.
[6] N. Kulischow, C. Ladasiu, R. Marschall, *Catal. Today* **2017**, *287*, 65–69.
[7] Y. Chen, X. Zhao, H. Ma, S. Ma, G. Huang, Y. Makita, X. Bai, X. Yang, *J. Solid State Chem.* **2008**, *181*, 1684–1694.
[8] H. Kato, A. Kudo, *Chem. Lett.* **1999**, *28*, 1207–1208.
[9] Y. Kobayashi, J. A. Schottenfeld, D. D. Macdonald, T. E. Mallouk, *J. Phys. Chem. C* **2007**, *111*, 3185–3191.
[10] T. Oshima, D. Lu, O. Ishitani, K. Maeda, *Angew. Chemie - Int. Ed.* **2015**, *54*, 2698–2702.
[11] M. Kato, Y. Imai, T. Kajita, Y. Takarabe, T. Minakawa, K. Nemoto, H. Tezuka, T. Noji, Y. Koike, *Mater. Sci. Eng. B* **2008**, *148*, 53–57.
[12] M. Fang, C. H. Kim, T. E. Mallouk, *Chem. Mater.* **1999**, *11*, 1519–1525.
[13] V. Thangadurai, P. Schmid-Beurmann, W. Weppner, *J. Solid State Chem.* **2001**, *158*, 279–289.
[14] M. Pilarski, R. Marschall, S. Gross, M. Wark, *Appl. Catal. B Environ.* **2018**, *227*, 349–355.
[15] T. Utkina, M. Chislov, O. Silyukov, A. Burovikhina, I. Alexeevna Zvereva, *J. Therm. Anal. Calorim.* **2016**, *125*, 281–287.
[16] T. Norby, M. Widerøe, R. Glöckner, Y. Larring, *Dalt. Trans.* **2004**, 3012–3018.
[17] X. Wang, J. Adhikari, L. J. Smith, *J. Phys. Chem. C* **2009**, *113*, 17548–17559.
[18] T. Mitsuyama, A. Tsutsumi, S. Sato, K. Ikeue, M. Machida, *J. Solid State Chem.* **2008**, *181*, 1419–1424.
[19] J. M. Jehng, I. E. Wachs, *Chem. Mater.* **1991**, *3*, 100–107.
[20] Y. Matsumoto, *J. Solid State Chem.* **1996**, *126*, 227–234.
[21] S.-H. Byeon, H.-J. Nam, *Chem. Mater.* **2000**, *12*, 1771–1778.
[22] L. Li, P. A. Salvador, G. S. Rohrer, *Nanoscale* **2014**, *6*, 24–42.

Supporting Information for

Tuning the Photocatalytic Activity of Layered perovskites Niobates by Controlled Ion Exchange and Hydration

Calin Ladasiu, Natalia Kulischow, Roland Marschall*

Dr. C. Ladasiu, N. Kulischow, Prof. R. Marschall
Institute of Physical Chemistry,
Justus-Liebig-University Giessen,
D-35392 Giessen, Germany
#present address: Department of Chemistry,
University of Bayreuth, 95447 Bayreuth, Germany
* Email: Roland.marschall@uni-bayreuth.de , ORCID: 0000-0002-1057-0459

Results and Discussion

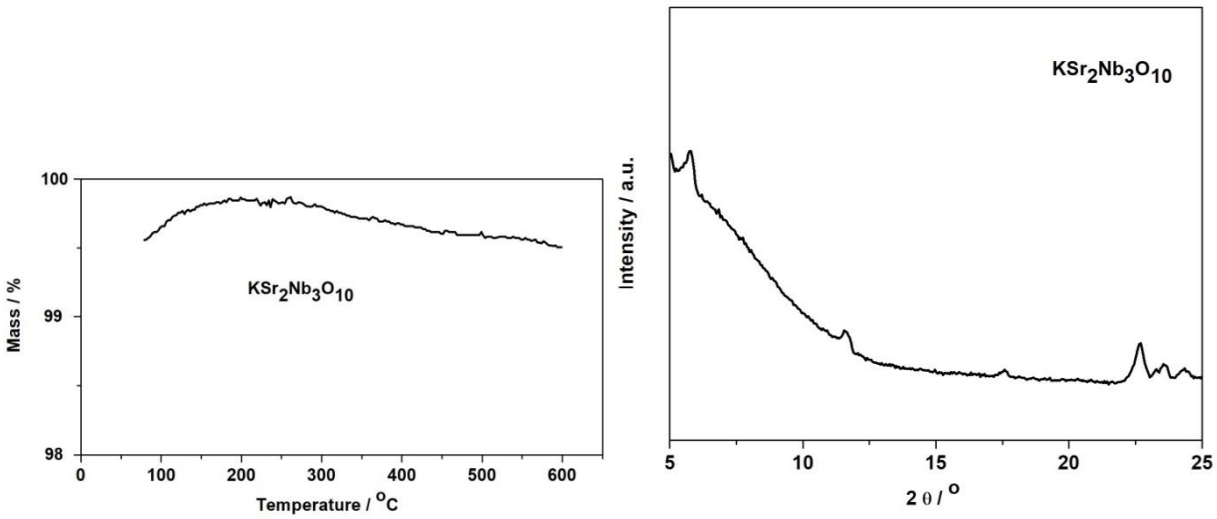

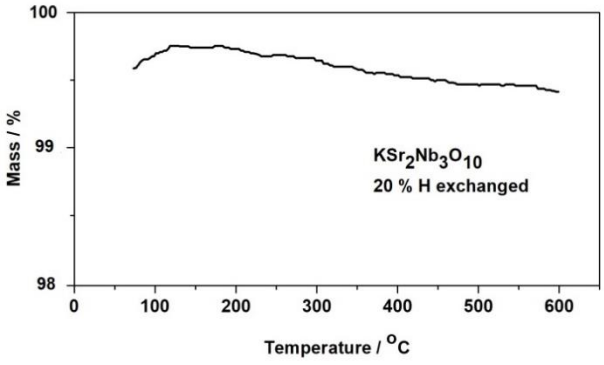
100
99
98
Mass / %
$KSr_2Nb_3O_{10}$
20 % H exchanged
0
100
200
300
400
500
600
Temperature / ^oC

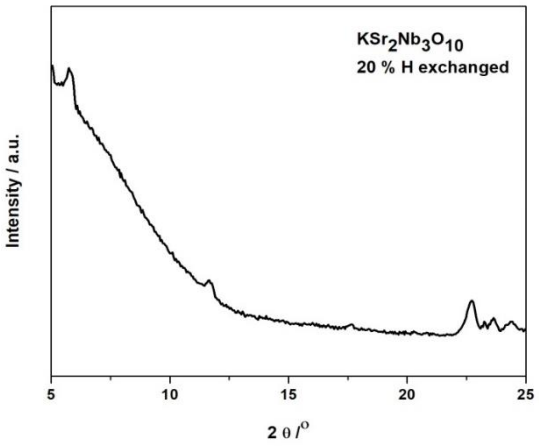
$KSr_2Nb_3O_{10}$
20 % H exchanged
Intensity / a.u.
5
10
15
20
25
2 θ /^{o}

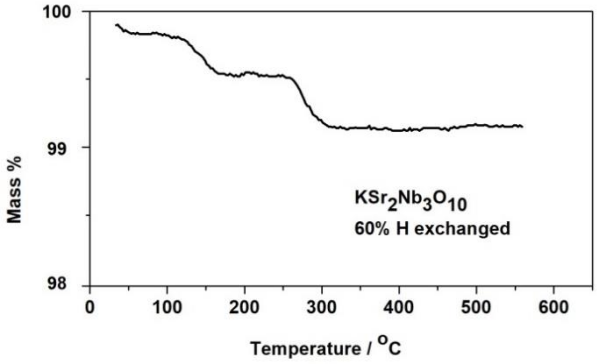
100
99
98
Mass %
$KSr_2Nb_3O_{10}$
60% H exchanged
0
100
200
300
400
500
600
Temperature / ^oC

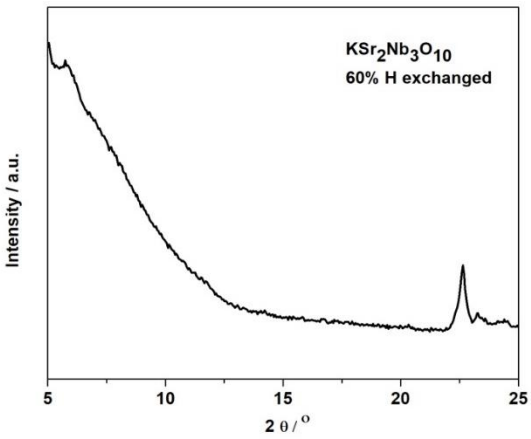
$KSr_2Nb_3O_{10}$
60% H exchanged
Intensity / a.u.
5
10
15
20
25
2 θ / ^{o}

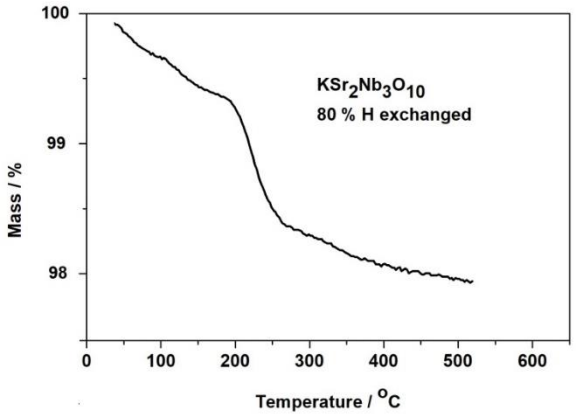
100
99
98
Mass / %
$KSr_2Nb_3O_{10}$
80 % H exchanged
0
100
200
300
400
500
600
Temperature / ^oC

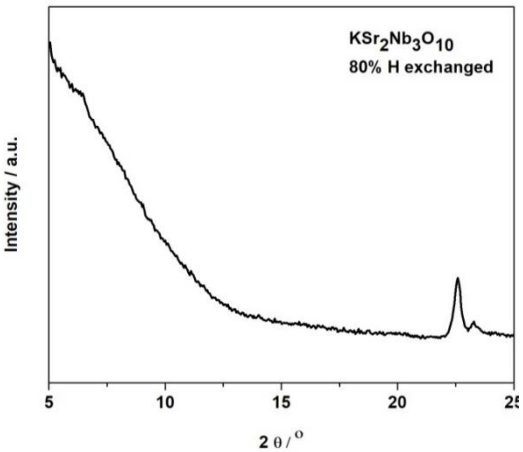
$KSr_2Nb_3O_{10}$
80% H exchanged
Intensity / a.u.
5
10
15
20
25
2 θ / ^{o}

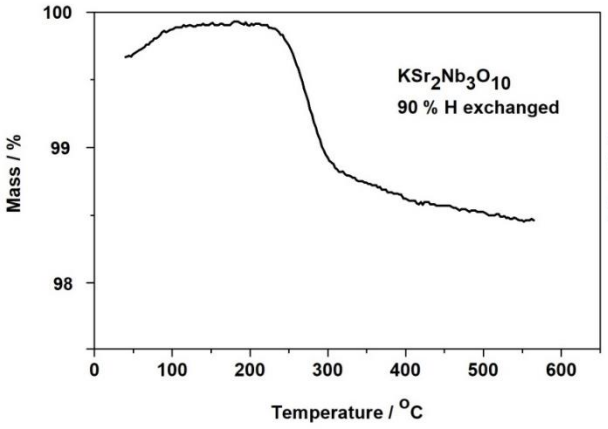
100
99
98
Mass / %
0
100
200
300
400
500
600
Temperature / °C
KSr2Nb3O10
90 % H exchanged

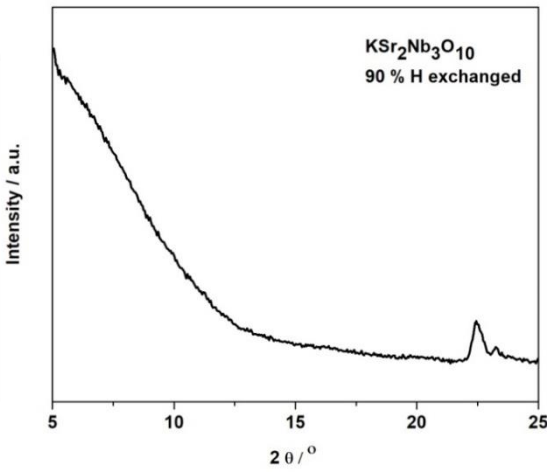
Intensity / a.u.
5
10
15
20
25
2 θ / °
KSr2Nb3O10
90 % H exchanged

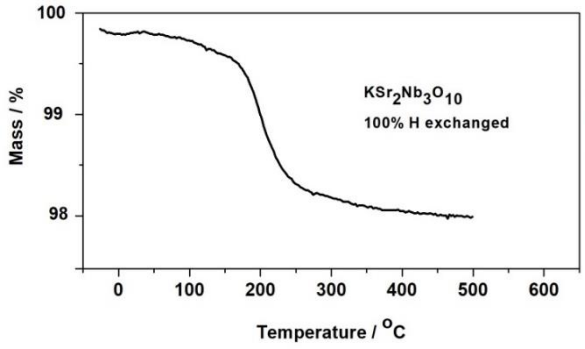
100
99
98
Mass / %
0
100
200
300
400
500
600
Temperature / °C
KSr2Nb3O10
100% H exchanged

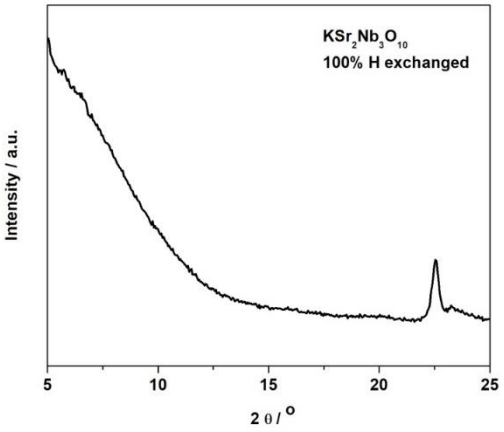
Intensity / a.u.
5
10
15
20
25
2 θ / °
KSr2Nb3O10
100% H exchanged

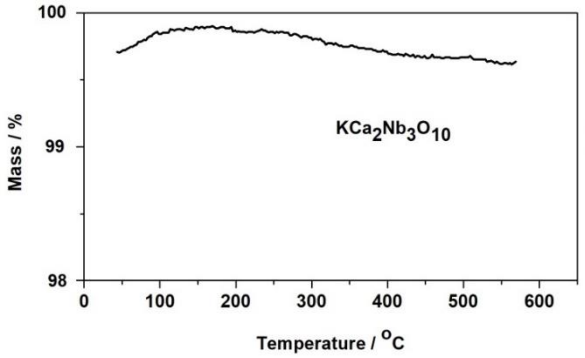
100
99
98
Mass / %
0
100
200
300
400
500
600
Temperature / °C
KCa2Nb3O10

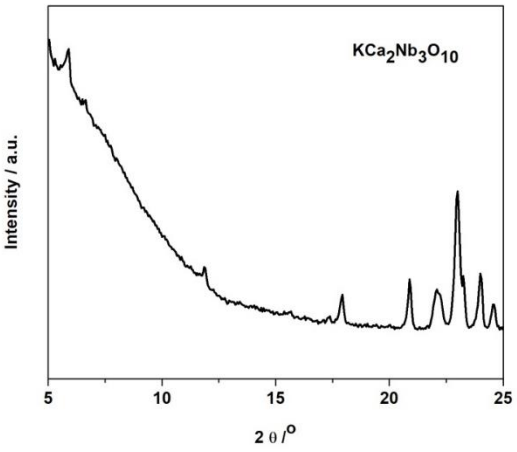
Intensity / a.u.
5
10
15
20
25
2 θ / °
KCa2Nb3O10

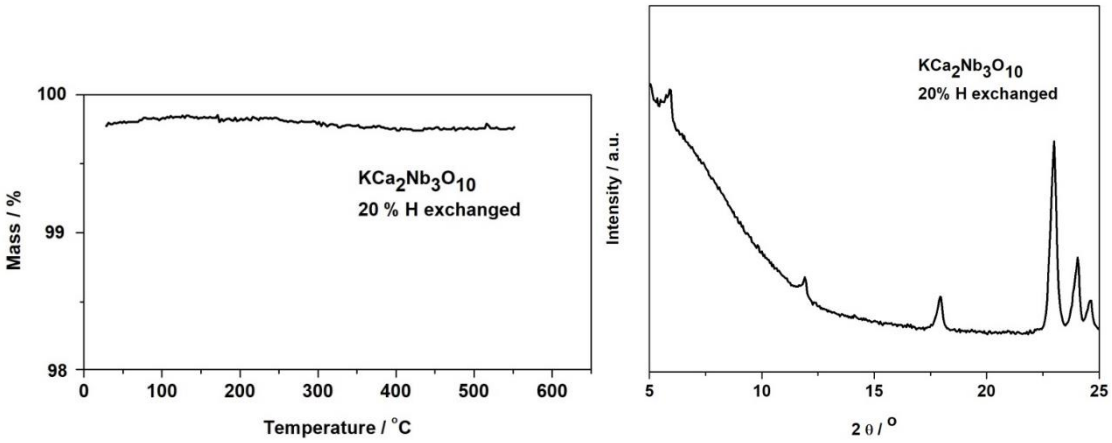
100
99
98
Mass / %
0
100
200
300
400
500
600
Temperature / °C
KCa2Nb3O10
20 % H exchanged
Intensity / a.u.
5
10
15
20
25
2 θ / °
KCa2Nb3O10
20% H exchanged

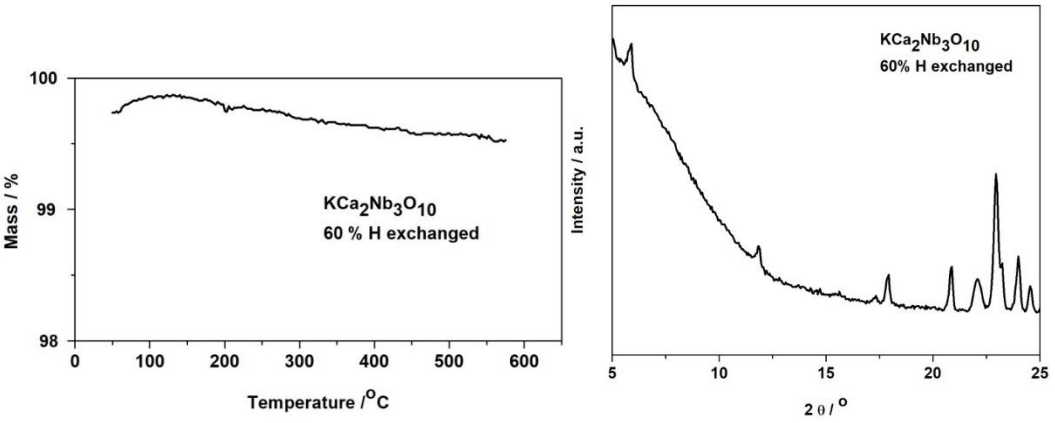
100
99
98
Mass / %
0
100
200
300
400
500
600
Temperature /°C
KCa2Nb3O10
60 % H exchanged
Intensity / a.u.
5
10
15
20
25
2 θ / °
KCa2Nb3O10
60% H exchanged

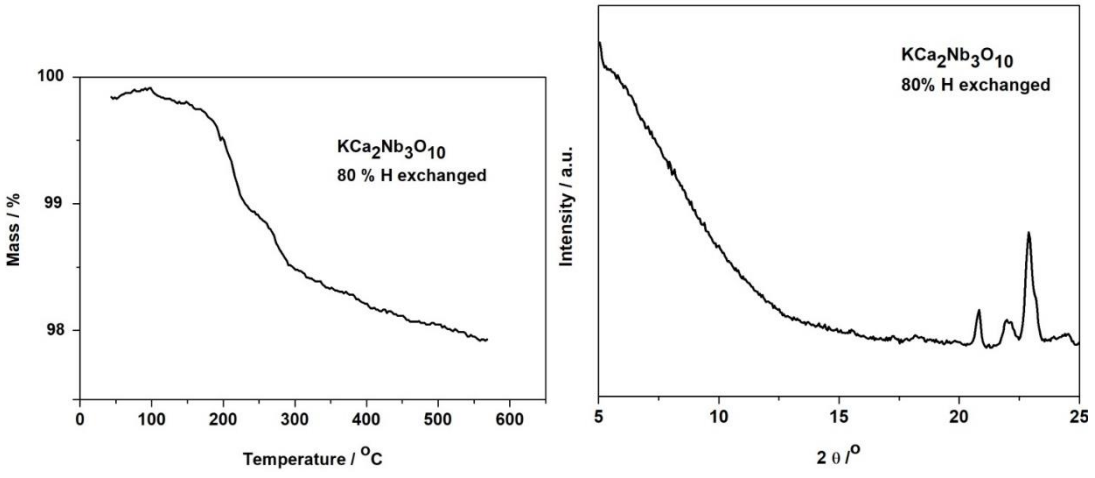
100
99
98
Mass / %
0
100
200
300
400
500
600
Temperature / °C
KCa2Nb3O10
80 % H exchanged
Intensity / a.u.
5
10
15
20
25
2 θ /°
KCa2Nb3O10
80% H exchanged

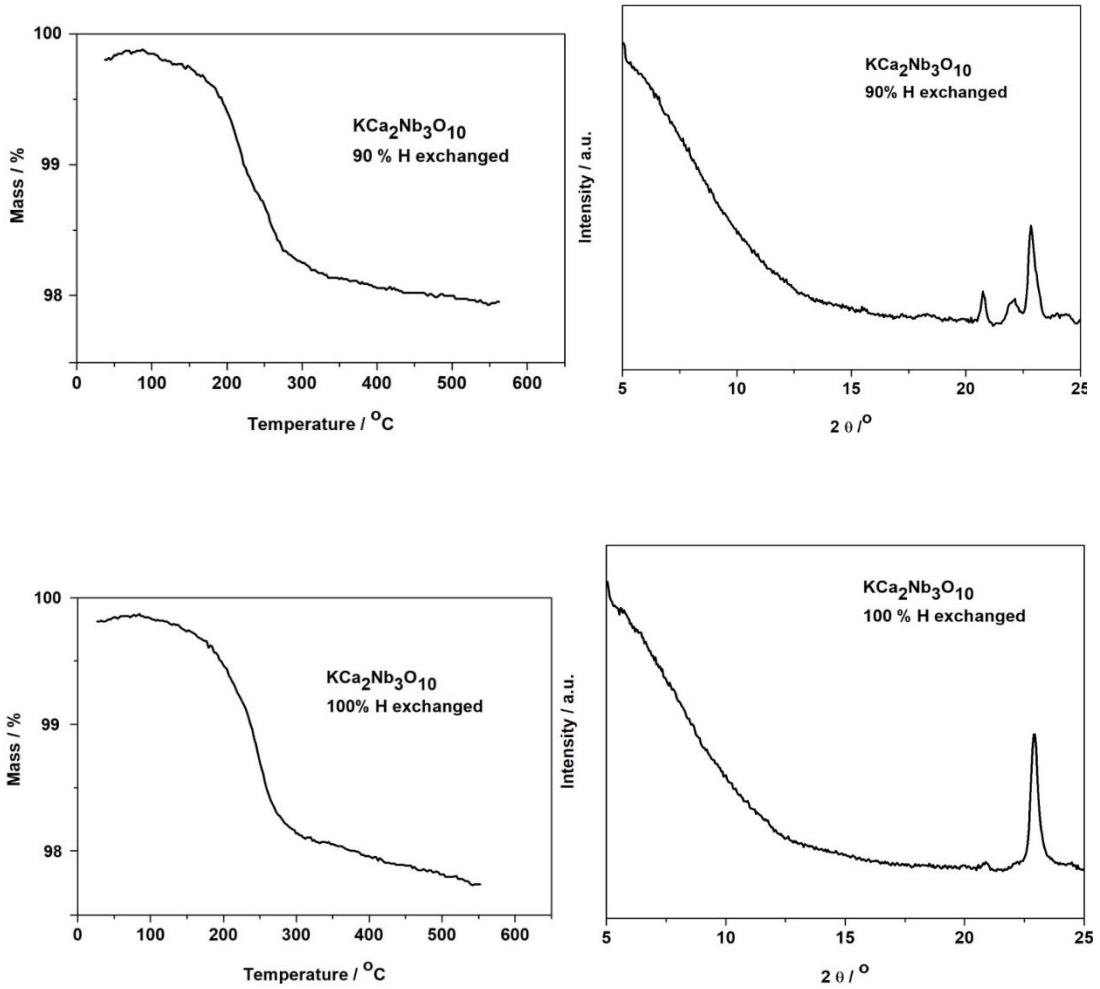

Figure S1: TGA (always left) and XRD patterns (always right) of indicated proton exchanged compounds

Table S1: Averaged atomic compositions of the niobium oxide compounds before and after proton exchange. Stirring of the compounds in 1M HNO_3 at room temperature for 30 min causes a proton exchange of 60 %. Heating the mixture up to 60 °C and stirring for 1 h results in 80 % exchange. Higher degree and the completion of exchange is achieved by stirring the mixture up to 18 h with intermediate solution exchange after every 3h.

degree of exchange	K	atomic % sigma	Sr	atomic % sigma	Nb	atomic % sigma
0 %	0.91	0.01	1.99	0.03	3	0.06
20 %	0.83	0.02	1.96	0.04	3	0.07
60 %	0.40	0.01	1.68	0.03	3	0.06
80 %	0.23	0.01	1.91	0.04	3	0.06
90 %	0.10	0.01	1.93	0.02	3	0.03
100 %	0.02	0.01	1.84	0.02	3	0.03
degree of exchange	**K**	**atomic % sigma**	**Ca**	**atomic % sigma**	**Nb**	**atomic % sigma**
0 %	0.93	0.05	1.83	0.05	3	0.09
20 %	0.80	0.02	2.09	0.04	3	0.08
60 %	0.39	0.02	2.03	0.02	3	0.05
80 %	0.23	0.02	1.86	0.02	3	0.05
90 %	0.13	0.05	1.88	0.04	3	0.05
100 %	0.02	0.01	1.97	0.02	3	0.05

Table S2: Water adsorption data for bulk and proton exchanged compounds.

Degree of proton exchange (%)	$KSr_2Nb_3O_{10}$		$KCa_2Nb_3O_{10}$	
	Adsorbed water (cm^3/g)	Water remaining after desorption (cm^3/g)	Adsorbed water (cm^3/g)	Water remaining after desorption (cm^3/g)
0	1.0	0.1	18.9	3.8
20	5.3	1.0	23.6	5.9
60	37.8	9.9	42.6	12.2
80	45.9	12.1	40.0	7.4
90	6.4	2.5	39.9	9.1
100	5.3	1.7	26.1	7.4

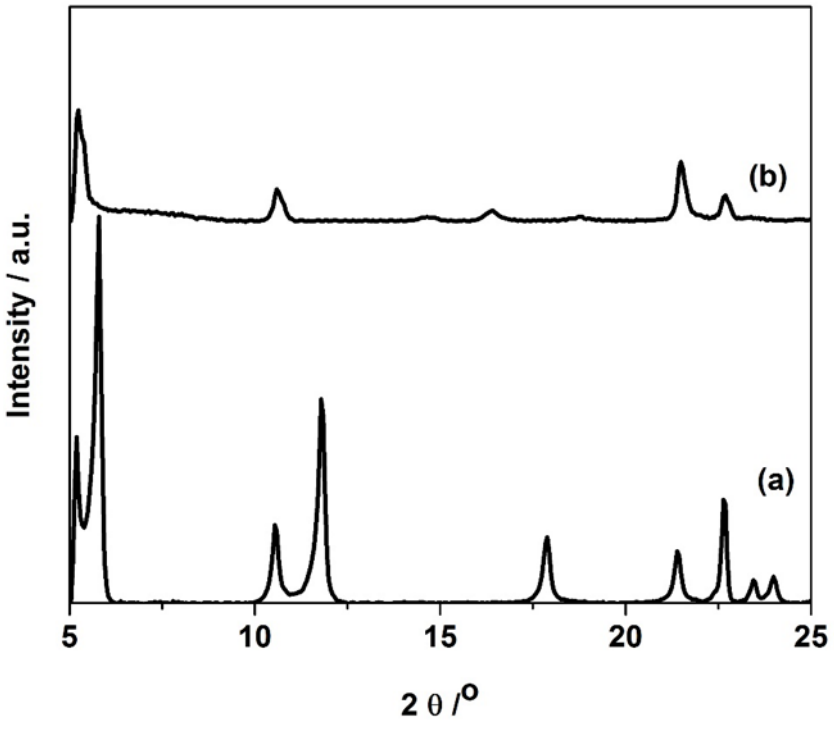

Figure S2: XRD patterns of $HSr_2Nb_3O_{10}$ before (a) and after (b) photocatalysis.

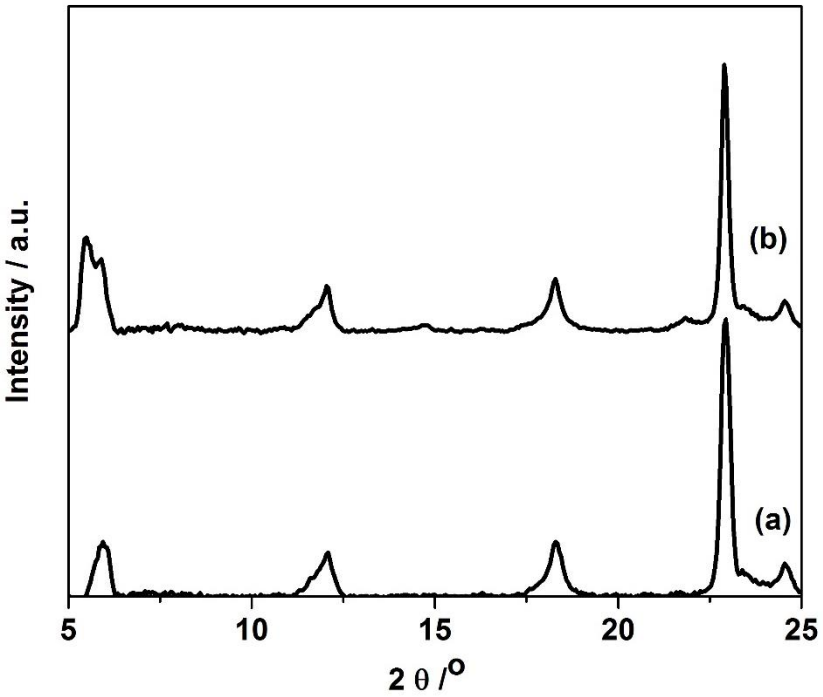

Figure S3: XRD patterns of $HCa_2Nb_3O_{10}$ before (a) and after (b) photocatalysis.